Vertically aligned carbon nanofiber-based field emission electron sources with an integrated focusing electrode

M. A. Guillorn,[a),b)] X. Yang,[b)] A. V. Melechko,[c)] D. K. Hensley, M. D. Hale, V. I. Merkulov, and M. L. Simpson[b)]
Molecular-Scale Engineering and Nanoscale Technologies Research Group, Oak Ridge National Laboratory, Oak Ridge, Tennessee 37831

L. R. Baylor and W. L. Gardner
Fusion Energy Division, Oak Ridge National Laboratory, Oak Ridge, Tennessee 37831

D. H. Lowndes
Thin Film and Nanostructured Materials Physics Research Group, Solid State Division, Oak Ridge National Laboratory, Oak Ridge, Tennessee 37831

(Received 10 May 2002; accepted 20 October 2003; published 24 December 2003)

We report on the design, fabrication, and initial characterization of vertically aligned carbon nanofiber-based microfabricated field emission devices with an integrated out-of-plane electrostatic focusing electrode. The potential placed on this electrode was found to have a profound impact on the diameter of the beam emitted from the device as observed on a phosphor screen. Aspects of the device fabrication process and device operation are discussed. The experimental results obtained are compared to a numerical simulation of device performance and found to be within good agreement. © *2004 American Vacuum Society.* [DOI: 10.1116/1.1633768]

I. INTRODUCTION

The design and fabrication of vacuum microelectronic devices based on field emission (FE) cathodes of various types have proven to be a fruitful area of research for many groups over the last three decades.[1] While most of this work has concentrated on the development of simple gated cathode electron sources, the construction of microfabricated FE devices with integrated electrostatic focusing lenses has become an area of increasing interest over the past eight years. Itoh and co-workers[2] reported an experimental realization of a microfabricated FE device of this type featuring a single out-of-plane focusing electrode stacked above the gate electrode and emitter. Since then, a number of papers have been published by various groups on this subject confirming the benefits of this design.[3–10] In particular, excellent control over the angular dispersion of the emitted beam can be achieved in an efficient manner without significantly degrading other aspects of device performance.[8,9]

The fabrication processes used to realize these devices and the focusing strategies employed in their design vary greatly with the exception of the material choice for the emitter tip. The bulk of this work has been performed using Si tips formed by etching and oxidation processes,[2–5,9,10] although refractory metal tips have also been explored.[7,8] Recently, the construction of nanostructured graphitic carbon for cold cathode FE devices has received a significant amount of attention by a number of groups.[11–17] This class of materials, including single- and multiwalled carbon nanotubes and carbon nanofibers, is believed to have some inherent advantages over Si and refractory metal-based FE cathodes resulting from their unique physical and chemical properties. In particular, observations of low threshold FE of electrons,[18] the ability to operate for extended periods of time in a moderate vacuum,[19,20] and high emission current density[21] have all been reported. These qualities demonstrate why these materials may prove to be a better choice for FE cathodes in some applications of integrated FE device technology.

For applications requiring the generation of a finely focused beam from a microscale source, for example, massively parallel electron-beam lithography (EBL),[22] the vertically aligned carbon nanofiber (VACNF) offers some additional advantages over other nanostructured graphitic carbon-based cathodes. In particular, the ability to construct devices with single VACNF cathodes greatly simplifies the design of integrated focusing and deflection optics and has a significant impact on the minimum achievable beam diameter. This stems from the fact that the location of the VACNF can be precisely controlled within the device structure. It follows that the emission site, presumed to be at or near the tip of the VACNF, can also be controlled with nanometer accuracy. This cannot be said of devices employing ensembles of nanotubes or nanofibers where multiple active emission sites are spread out over an entire micron-scale cathode.

In this article, we report on the fabrication and initial characterization of FE electron sources with an integrated focusing electrode that use a single VACNF as the electron emitter. These devices include a single out-of-plane coaxial focusing electrode stacked above the gate electrode to provide a local electrostatic refocusing of the emitted electron beam. These results show that the presence of this electrode has a marked effect on the performance of the device. The fabrication process used in this work is discussed in detail

[a)]Author to whom correspondence should be addressed; electronic mail: guillornma@ornl.gov
[b)]Also with the Department of Materials Science and Engineering, University of Tennessee, Knoxville, Tennessee 37996.
[c)]Also with the Department of Electrical and Computer Engineering, University of Tennessee, Knoxville, Tennessee 37996.

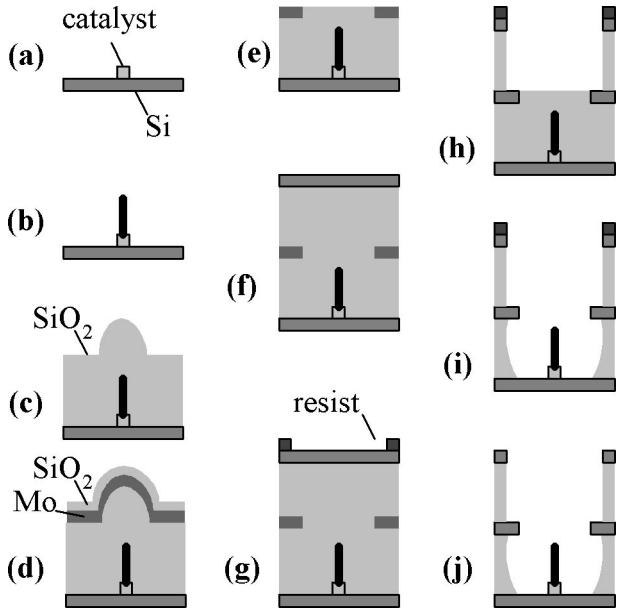

FIG. 1. Overview of the fabrication process used to realize the VACNF-based FE devices with integrated focusing electrodes.

along with elements of the operating characteristics. A numerical simulation of the device is presented and found to be in good agreement with the experimentally observed results, confirming that an actual refocusing of the emitted electron beam is achieved.

II. DEVICE FABRICATION

A diagram of the fabrication process used in this work is shown in Fig. 1. Whole 4 in. diameter 1–10 Ω cm *n*-type Si wafers were used as substrates throughout this work. Conventional high-resolution EBL and liftoff pattern transfer were used to define catalyst sites for the deterministic growth of VACNF and alignment marks for subsequent lithographic patterning processes [Fig. 1(a)]. The catalyst site pattern consisted of 100 nm diameter circles. These patterns were metallized with 100 Å of Ti followed by 100 Å of Ni deposited by electron-beam physical vapor deposition (PVD). The Ti layer was deposited between the Ni catalyst and Si substrate to prevent catalyst silicide formation at the moderately high growth temperature of approximately 650 °C.

VACNF growth was performed in a hot cathode dc plasma enhanced chemical vapor deposition (PECVD) growth system as previously described.[23] After evacuating the growth system to a suitable base pressure, the temperature of the cathode was increased, ammonia (NH_3) was introduced into the chamber, and a dc glow discharge plasma was initiated. As a result of this treatment, catalyst nanoparticles were formed from the deposited circular catalyst pattern.[23] For Ni patterns with the diameter and thickness used here, only a single nanoparticle was formed at each patterned site. These nanoparticles act as the necessary seeds for the catalytic growth of isolated VACNFs. After the preetching step, acetylene (C_2H_2) was introduced into the chamber during continued operation of the NH_3 plasma beginning the VACNF growth [Fig. 1(b)]. The NH_3 and C_2H_2 gas flows used in this work were 80 sccm and 60 sccm, respectively. The total gas pressure during the growth was ~2.5 Torr. Postgrowth imaging of VACNF was carried out using a Hitachi S4700 high-resolution scanning electron microscope (SEM). VACNF produced for this work were found to have a radius of curvature of 15 nm and a height of 1 μm, on average.

Following characterization of the VACNF material, a 1 μm thick conformal layer of SiO_2 was deposited onto the substrates using a silane-based rf PECVD process [Fig. 1(c)]. A 150 nm thick layer of Mo was then deposited onto the substrates using electron-beam PVD followed by a 250 nm thick layer of SiO_2 deposited by rf PECVD [Fig. 1(d)]. The wafers were then planarized using a chemical–mechanical polishing technique, removing the conformal film stack surrounding the VACNF tips and forming a self-aligned gate aperture [Fig. 1(e)]. VACNF-based gated cathodes fabricated using this process were reported in a previous work.[24] A second layer of 1 μm thick SiO_2 was deposited onto the substrates to serve as an insulating layer between the gate and focus electrodes. The focus electrode was then metallized and patterned using identical processing as the gate electrode [Fig. 1(f)]. Photoresist was applied to the substrate and photolithography was used to define the electrode apertures aligned to the buried VACNF emitter [Fig. 1(g)]. Using the resist as a mask, the aperture was etched into the focus electrode layer using a CF_4/SF_6 reactive ion etch (RIE). This etch was followed by removal of the upper oxide layer by a CHF_3/O_2 RIE. After removing this layer, the lower SiO_2 layer was removed using a buffered HF solution [Fig. 1(h)]. Finally, the remaining resist was removed from the substrates using acetone and ultrasonic agitation [Fig. 1(i)].

A schematic of the device is shown in Fig. 2(a) showing all typical relevant dimensions. SEM micrographs of a completed device are shown at 30° and normal incidence in Figs. 2(b) and 2(c), respectively. It is clear from the latter image that misalignment between the VACNF and the center of the electrode apertures can be minimized using this fabrication technique. However, nonuniformities in the VACNF growth can result in significant misalignment of the gate and focus electrodes. This occurred in less than half of the devices examined in this work.

III. EXPERIMENTAL RESULTS

Field emission measurements were carried out in a chamber evacuated to a base pressure of 10^{-6} Torr to simulate operation in less than ideal environments. A conductive glass anode coated with a phosphor (p22, Kimball Physics) was placed 6.7 mm directly above the Si substrate containing the VACNF-based FE devices. Keithley Instruments (KI) model 2410 dc source-measure units (SMU) were used to perform all electrical measurements. For each device under test, a separate SMU was connected to the cathode, gate, focusing electrode, and anode. During all device testing, the voltage on the gate electrode, V_g, was held at 0 V, and the voltage on

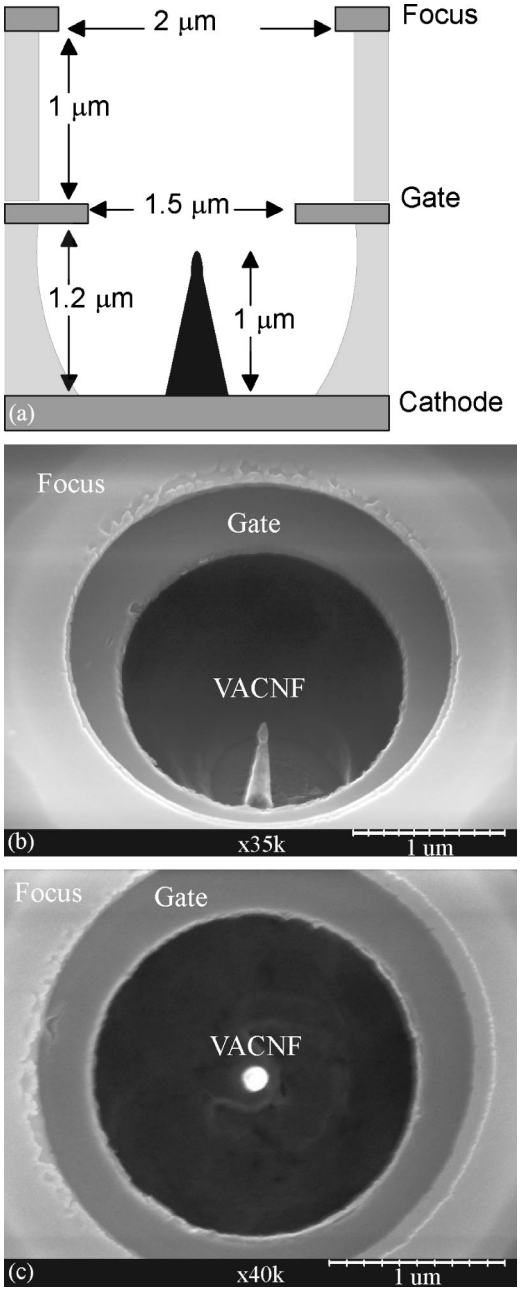

FIG. 2. SEM micrograph taken at 35° from normal incidence of a VACNF-based FE device with an integrated focusing electrode.

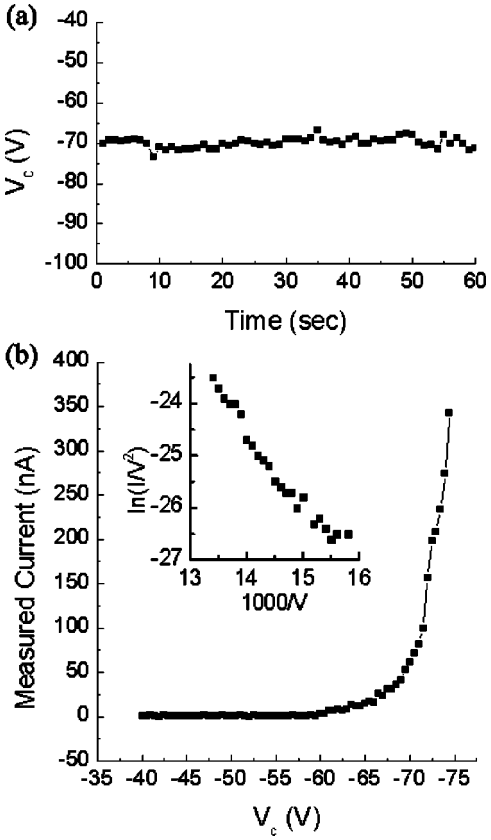

FIG. 3. (a) V_c required to source 50 nA of current over an interval of 60 s following device conditioning where $V_f = V_g = 0$ V. (b) I_a measured during an FE $I-V$ curve of a single device where $V_f = V_g = 0$ V. Inset: Corresponding Fowler–Nordheim plot of the data shown in (b).

the anode, V_a, was fixed at 1 kV. The anode, gate, focus electrode, and substrate currents were measured as the voltage on the cathode, V_c, and focus electrode, V_f, were varied independently from 0 V to -80 V. Only individual devices containing a single VACNF emitter were analyzed.

Devices were conditioned by using the KI 2410 connected to the cathode to vary V_c such that a 50 nA beam was emitted from the VACNF. During this process, V_f and V_g were set to 0 V [refer to Fig. 3(a)]. Once reasonably stable operation of the device was achieved, FE current versus voltage, current–voltage ($I-V$), data was obtained by sweeping the cathode voltage from 0 to -75 V while setting V_g and V_f at 0 V [refer to Fig. 3(b)].

The focusing performance of the device was investigated by capturing the image of the emitted electron beam on the phosphor anode using a color digital video camera. Images of the beam taken at $V_c = -80$ V, $V_g = 0$ V, $V_f = 0$ V, -60 V, and -75 V are shown in Figs. 4(a)–4(c), respectively. Each image was processed by first inverting the red–green–blue (RGB) image followed by converting it to gray-scale. No further image processing was performed. The emitted current for these tests ranged between 500 nA for $V_f = 0$ V and 100 nA for $V_f = -75$ V. This decrease in current is attributed to the reduction in field at the emitter tip caused by the decrease in V_f. Attempts to operate the devices at focusing voltages lower than -75 V lead to over focusing of the beam. Under these conditions, more than 95% of the emitted beam was intercepted by the gate electrode and no image was visible on the phosphor anode. At $V_f = -75$ V, less than 1% of the emitted beam was collected by the gate and focus electrodes. In contrast, 3%–5% of the emitted current was routinely collected by the focus electrode for $V_f = 0$ V.

IV. SIMULATION OF DEVICE PERFORMANCE

It is clear from Fig. 4 that a change in V_f corresponds to a change in the diameter of the emitted beam. As mentioned above, the beam current is dependent on the value of V_g and V_f due to their influence on the electric field at the VACNF

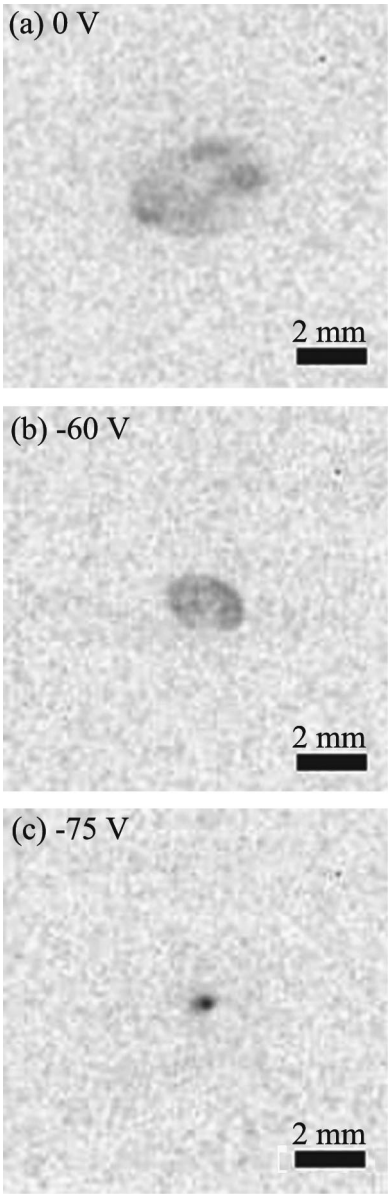

FIG. 4. Images of the electron beam emitted from a single operating device for V_f of (a) 0 V, (b) -60 V, and (c) -75 V displayed on a phosphor imaging anode. The images were obtained using a color digital video camera and exported as RGB images. Each image was processed by first inverting the RGB image followed by converting it to grayscale. No further image processing was performed.

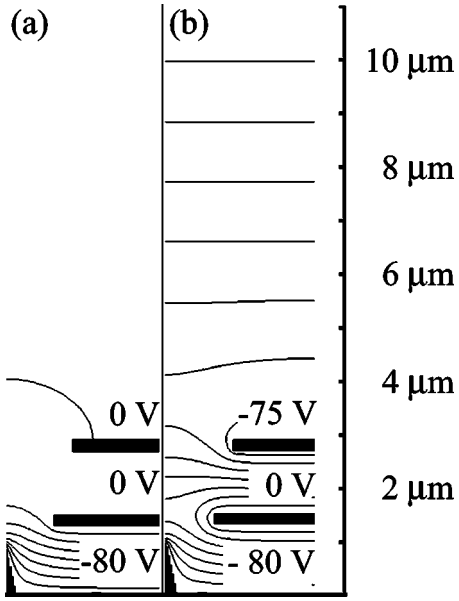

FIG. 5. Equipotential plots for the tested device for (a) $V_f=0$ V and (b) $V_f=-75$ V, where $V_g=0$ V, $V_c=-80$ V, and $V_a=1$ kV. The contour closest to the cathode in each plot represents -70 V. Contours were plotted in increments of 10 V.

tip. Increasing the intensity of the electric field results in a larger emission current caused, in part, by an increase in the area over which electron emission can occur. Consequently, the angular distribution of the emitted beam about the tip also increases. These changes in operational beam current manifest themselves as variations in the size and shape of the emitted beam observed on an imaging anode. This is true regardless of the use of a focusing electrode.

In order to examine whether focusing of the emitted beam was responsible for the behavior observed in Fig. 4, the experimentally obtained results were compared against a numerical simulation of the tested device. Simulations were conducted using a commercially available software package, LORENTZ 2D from Integrated Engineering Software. This program uses the boundary element method (BEM) and is designed for the purpose of ray tracing of charged particles. The BEM technique solves for the charge distribution on the boundaries of a user-defined structure based on an integral formulation. The electric field is computed from this charge distribution and is subsequently used to perform ray tracing of charged particles. This computation assumes cylindrical symmetry about the z axis.

The simulation model presented in this work was based on the geometry of the device structure used to produce the images shown in Fig. 4. The dimensions agree with those shown in Fig. 2(a) with the exception of the diameter of the gate and focus electrode apertures. These values were measured in an SEM as 1.6 and 2.2 μm, respectively. Figures 5(a) and 5(b) show the equipotential lines calculated from the charge distribution on the boundaries present in the device for $V_f=0$ V and -75 V, respectively. V_c, V_g, and V_a were fixed at -80, 0, and 1000 V, respectively, in both calculations.

A series of simulations was conducted to determine the angular distribution of the electron emission over the emitter tip required to produce the experimentally observed value of the emitted beam diameter for each operating condition. For a value of $V_f=0$ V, emission distributed over a 60° half-angle produced the experimentally observed 3.9 mm diameter beam. These conditions also produced rays that were intercepted by the focusing electrode, agreeing with experimental observations of focus electrode current at this operating point. The results of these simulations are shown in Figs. 6(a) and 6(b). For a value of $V_f=-75$ V, emission distributed over a 15° half-angle produced the experimentally observed 0.28 mm diameter beam. The results of these simu-

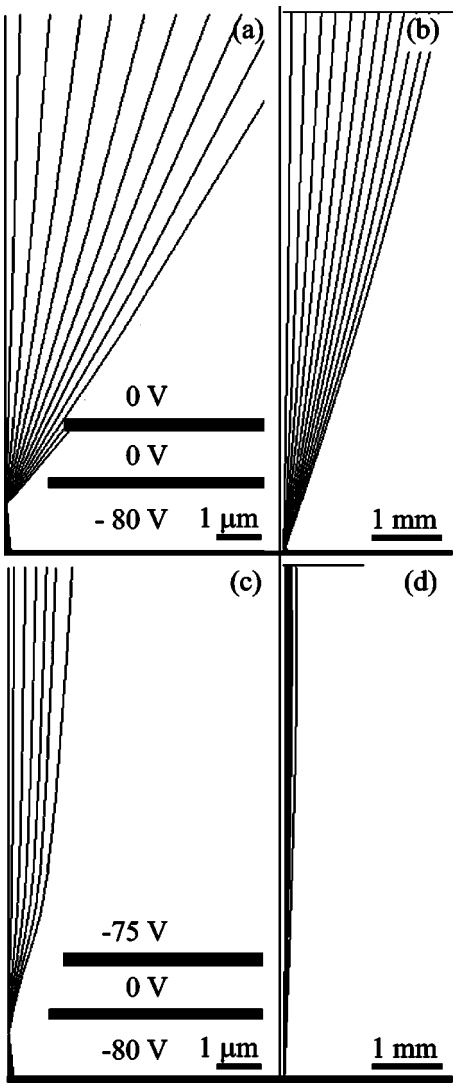

FIG. 6. Simulation of device performance showing electron trajectories plotted in the near cathode region, (a) and (c), and at a target biased at 1 kV placed 6.7 mm away from the cathode, (b) and (d). The simulation shown in (a) and (b) assumed a half angle of emission of 60°; the case shown in (c) and (d) assumed a half angle of emission of 15°.

lations are shown in Figs. 6(c) and 6(d). It is worth noting that use of a 15° half-angle of emission for the $V_f = 0$ V case produced a beam 0.93 mm in diameter with no trajectories intercepting the focus electrode. This illustrates the point that while the emitted beam diameter is highly dependent on the angular distribution of electron emission at the VACNF tip, it cannot completely account for the experimentally observed behavior.

V. CONCLUSION

In this article, we have demonstrated the fabrication and operation of microfabricated electron gun structures with integrated focusing electrodes using a single VACNF as the FE cathode. The performance of the integrated focusing electrode was investigated and found to have a significant impact on the beam diameter observed on a phosphor screen. This result is in good agreement with numerical simulations of device performance presented in this article revealing that true refocusing of the electron beam is occurring.

The primary limitation of the current embodiment of this device is lack of device-to-device uniformity. Small differences in the VACNF geometry translate into variations in the gate electrode aperture shape and position. Better control over the VACNF growth process can eliminate these problems. This subject remains an active area of research within our own research group and several others.

ACKNOWLEDGMENTS

The authors wish to thank P. H. Fleming and T. R. Subich for their assistance in sample preparation, and F. Rizzo, P. E. Zonnes, and B. Ilic for helpful discussions. This work was funded by DARPA under Contract No. 1868HH26X1 and by the Laboratory Directed Research and Development Program of the Oak Ridge National Laboratory (ORNL). ORNL is managed by UT-Battelle, LLC, for the U.S. Department of Energy under Contract No. DE-AC05-00OR22725. This work was performed in part at the Cornell Nanofabrication Facility (a member of the National Nanofabrication Users Network) that is supported by the National Science Foundation under Grant No. ECS-9731293, its users, Cornell University, and industrial affiliates.

[1]D. Temple, Mater. Sci. Eng., R. **24**, 185 (1999).
[2]J. Itoh, Y. Tohma, K. Morikawa, S. Kanemaru, and K. Shimizu, J. Vac. Sci. Technol. B **13**, 1968 (1995).
[3]Y. Toma, S. Kanemaru, and J. Itoh, J. Vac. Sci. Technol. B **14**, 1902 (1996).
[4]J. H. Lee, Y. H. Song, S. Y. Kang, S. G. Kim, and K. I. Cho, J. Vac. Sci. Technol. B **16**, 811 (1998).
[5]A. Hosono, S. Kawabuchi, S. Horibata, S. Okuda, H. Harada, and M. Takai, J. Vac. Sci. Technol. B **17**, 575 (1999).
[6]D. Nicolaescu, V. Filip, and J. Itoh, J. Vac. Sci. Technol. B **19**, 892 (2001).
[7]D. Li and K. Zhang, J. Vac. Sci. Technol. B **19**, 1820 (2001).
[8]L. Dvorson and A. I. Akinwande, J. Vac. Sci. Technol. B **20**, 53 (2002).
[9]L. Dvorson, I. Kymissis, and A. I. Akinwande, J. Vac. Sci. Technol. B **21**, 486 (2003).
[10]N. N. Chubun, A. G. Chakhovskoi, M. Hajra, and C. E. Hunt, J. Vac. Sci. Technol. B **21**, 483 (2003).
[11]X. Xu and G. R. Brandes, Mater. Res. Soc. Symp. Proc. **509**, 107 (1998).
[12]Q. H. Wang, M. Yan, and R. P. H. Chang, Appl. Phys. Lett. **78**, 1294 (2001).
[13]Y. H. Lee, Y. T. Jang, D. H. Kim, J. H. Ahn, and B. K. Ju, Adv. Mater. (Weinheim, Ger.) **13**, 479 (2001).
[14]D. S. Hsu and J. Shaw, Appl. Phys. Lett. **80**, 118 (2002).
[15]Y. S. Choi *et al.*, Appl. Phys. Lett. **82**, 3565 (2003).
[16]G. Pirio, P. Legagneux, D. Pribat, K. B. K. Teo, M. Chhowalla, G. A. J. Amaratunga, and W. I. Milne, Nanotechnology **13**, 1 (2001).
[17]M. A. Guillorn, A. V. Melechko, V. I. Merkulov, E. D. Ellis, C. L. Britton, M. L. Simpson, D. H. Lowndes, and L. R. Baylor, Appl. Phys. Lett. **79**, 3506 (2001).
[18]W. A. de Heer, A. Chatelain, and D. Ugaarte, Science **269**, 1179 (1995).
[19]F. S. Baker, A. R. Osborn, and J. Williams, J. Phys. D **7**, 2105 (1974).
[20]K. A. Dean and B. R. Chalamala, Appl. Phys. Lett. **75**, 3017 (1999).
[21]L. R. Baylor, V. I. Merkulov, E. D. Ellis, M. A. Guillorn, D. H. Lowndes, A. V. Melechko, M. L. Simpson, and J. H. Whealton, J. Appl. Phys. **91**, 4602 (2002).
[22]L. R. Baylor *et al.*, J. Vac. Sci. Technol. B **20**, 2646 (2002).
[23]V. I. Merkulov, D. H. Lowndes, Y. Y. Wei, G. Eres, and E. Voelkl, Appl. Phys. Lett. **76**, 3555 (2000).
[24]M. A. Guillorn, A. V. Melechko, V. I. Merkulov, D. K. Hensley, M. L. Simpson, and D. H. Lowndes, Appl. Phys. Lett. **81**, 3660 (2002).